J Mater Sci (2007) 42:1972–1983
DOI 10.1007/s10853-006-0739-7

NONSTOICHIOMETRIC COMPOUNDS

Oxygen transport in $La_{2-x}Sr_x NiO_{4+\delta}$: membrane permeation and defect chemical modelling

M. Schroeder · M.-A. Dragan

Received: 24 March 2006 / Accepted: 28 July 2006 / Published online: 3 February 2007

Abstract We describe a defect and transport model for acceptor doped $La_{2-x}Sr_xNiO_{4+\delta}$ with the layered K_2NiF_4 structure. The model includes mobile oxygen interstitials in the rocksalt layers and oxygen vacancies in the perovskite layers of the crystal structure. Based on fits of literature data of the deviation from stoichiometry, defect concentrations have been calculated for $La_{1.5}Sr_{0.5}NiO_{4+\delta}$ as a function of $p(O_2)$ for 1,073–1,223 K. Application of the transport model to oxygen permeation data obtained in this work clearly indicates that the oxygen transport in $La_{1.5}Sr_{0.5}NiO_{4+\delta}$ is primarily governed by migration of mobile oxygen interstitials. According to the model calculations, a significant contribution of vacancy migration to the oxygen permeation process is to be expected only for oxygen partial pressures lower than 10^{-5} bar at 1,223 K and even lower partial pressures at 1,073 and 1,173 K. As yet, permeation data are not available for such low partial pressures, which is why oxygen migration via vacancies could neither be confirmed nor ruled out.

Introduction

Layer-structured oxides $La_{2-x}Sr_xNiO_{4+\delta}$ with the perovskite-like K_2NiF_4 structure have been widely studied since the discovery of high-temperature superconductivity in the isostructural oxide $La_{2-x}Ba_xCuO_4$ [1]. Whereas investigations were mainly focussed on magnetic [2–7] and electronic properties [8–11] in the low temperature regime below 400 K, it became evident in the past decade that $La_{2-x}Sr_xNiO_{4+\delta}$ is, due to its mixed ionic electronic conduction, an interesting candidate for high-temperature applications such as SOFC electrodes and ceramic membranes for partial oxidation of hydrocarbons [12–16].

The parent compound $La_2NiO_{4+\delta}$ belongs to the Ruddlesden-Popper series which has the general composition $A_{n+1}B_nO_{3n+1}$ (n = 1, 2, 3, ...). The crystal structures of this series show a close proximity to the perovskite structure as they are obtained by inserting rocksalt-type AO sheets between blocks consisting of n ABO_3 perovskite-type layers. In the case of the K_2NiF_4 structure (n = 1), AO layers and ABO_3 layers are alternately stacked in the crystallographic c direction (Fig. 1).

A different representation of the K_2NiF_4 structure is based on an alternate stacking of La_2O_2 double layers and BO_2 sheets. By assuming partial charge separation between these layers ($La_2O_2^{y+}/BO_2^{y-}$), one may anticipate that defects with negative charge are preferentially accommodated in the La_2O_2 layers, whereas defects with positive charge reside in the BO_2 sheets. In fact, it was found that $La_2NiO_{4+\delta}$ can accommodate considerable amounts of excess oxygen. Neutron diffraction studies revealed that this excess oxygen is hosted in the form of oxygen interstitial defects in the La_2O_2 rocksalt layers [17, 18]. The defect site is coordinated tetrahedrally both by Lanthanum ions and apical oxygen ions, as indicated in Fig. 1. Values of δ as large as +0.25 have been reported [19]. The wide range of oxygen stoichiometry provides for a rich phase chemistry at low temperatures [20–23], whereas

M. Schroeder (✉) · M.-A. Dragan
Institute of Physical Chemistry, RWTH Aachen,
Landoltweg 2, 52056 Aachen, Germany
e-mail: schroeder@rwth-aachen.de

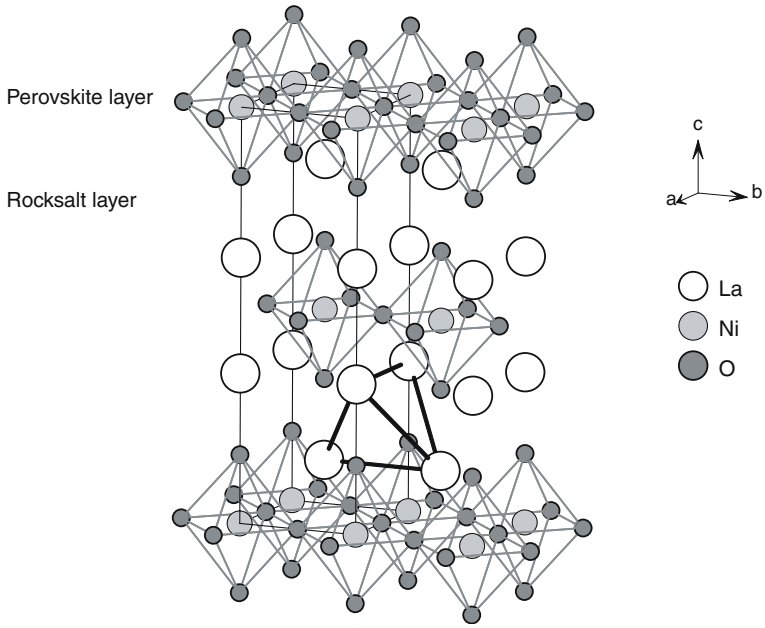

Fig. 1 High-temperature tetragonal I4/mmm form of the K_2NiF_4 structure. Thick bonds indicate the tetrahedral lanthanum coordination around an interstitial lattice site

at $T > 770$ K a tetragonal structure with I4/mmm symmetry is found over the entire range of stoichiometry. $La_2NiO_{4+\delta}$ is a p-type semiconductor at lower temperatures and undergoes a semiconductor to metal transition with increasing temperature [24]. Charge compensation of the excess oxygen occurs predominantly by formation of electron holes. According to static lattice simulations [25] carried out for $La_2NiO_{4+\delta}$, the preferred extrinsic disorder mechanism is the formation of doubly charged oxygen interstitial ions $O_{i}^{''}$ (subscript i denotes the interstitial sublattice) and electron holes localized on nickel ions in the NiO_2 sheets. The most favourable intrinsic disorder process is reported to be the formation of Frenkel pairs of oxygen interstitials and oxygen vacancies, the latter being accommodated in equatorial sites of the perovskite structured layers [25, 26]. If these vacancies were mobile, they might contribute to oxygen migration inside the perovskite layers, and oxygen transfer across the layers should be observed. This is in fact supported by a recent study on the orientation dependence of oxygen tracer diffusion in single-crystalline $La_2NiO_{4+\delta}$ [27] at temperatures between 723 K and 1,173 K. Oxygen diffusion was observed not only along the (*a*,*b*) planes of the structure but also parallel to the c direction, although perpendicular to the layers the diffusion was found to be 1–2 orders of magnitude slower than parallel to the layers.

Acceptor doping of $La_2NiO_{4+\delta}$ with earth-alkali elements increases the electrical conductivity and decreases the oxygen excess. A thermogravimetric investigation of $La_{2-x}Sr_xNiO_{4+\delta}$ with various dopant contents [15] indicates that these compounds are always oxygen excessive under oxidizing conditions. However, under reducing conditions, a transition from oxygen excess to oxygen deficiency is found for heavily doped $La_{1.5}Sr_{0.5}NiO_{4+\delta}$ at a temperature of 1,223 K, which hints on formation of a significant amount of oxygen vacancies.

In this paper we report about a study of the oxygen transport in $La_{1.5}Sr_{0.5}NiO_{4+\delta}$ subjected to an oxygen potential gradient. Experimental data were obtained by a membrane permeation technique. The results are discussed by means of a model of the defect chemistry and the oxygen transport in acceptor doped $La_{2-x}Sr_xNiO_{4+\delta}$. The model includes both oxygen interstitials in the La_2O_2 layers and oxygen vacancies in the perovskite layers as structural defects. The significance of oxygen vacancies for the oxygen transport process is discussed.

Experimental details

Samples of $La_{1.5}Sr_{0.5}NiO_{4+\delta}$ were synthesized by a sol–gel method starting from aqueous solutions of nitrates of lanthanum, strontium and nickel in the appropriate molar ratios, which were mixed with citric acid and polyethylene glycol to promote chelate formation and polyesterification. The resulting gel was dried and calcined at 1,273 K in air for 24 h, followed by a second calcination step at 1,473 K for 24 h. The powders were then ground, pelletized, heated for 50 h at 1,523 K, and furnace-cooled. The sintered pellets had a diameter of

20 mm and were 1.3 mm thick. Both pellet faces were ground and polished to a surface roughness of < 1.5 μm.

Fractions of the synthesized oxide powders were characterized by X-ray diffraction using a STADI P diffractometer (STOE) with monochromated CoKα radiation and a position sensitive detector. Intensity data were collected for 1 second at each 0.01° step width over a 2θ range from 10° to 90°. The composition of the pellets was determined by energy dispersive X-ray analysis using an INCA energy EDX system (Oxford) mounted on a LEO electron microscope.

The pellets were then used as membranes for measurements of the permeation flux of oxygen in a gradient of oxygen chemical potential. Each membrane was mounted between two alumina tubes. Between the membrane and the tubes, ring-shaped glass gaskets were placed to prevent leakage from one gas compartment to the other. To enhance the sealing, the outer circumference of the membrane was painted with a glass-powder slurry. The membrane and part of the alumina tubes were heated by an electrically powered tube furnace. The experimental set-up is shown in Fig. 2.

By flowing gases with different oxygen partial pressures along either membrane surface, a gradient of oxygen chemical potential across the membrane was established. Air was used as feed gas, and argon served as sweep gas to pick up the permeated oxygen. By varying the sweep gas volume flow rate, the oxygen partial pressure on the sweep gas side was adjusted. The gas flow rates were controlled and measured by mass flow controllers and a mass flow meter, respectively. Any oxygen transferred across the membrane from the feed gas side to the permeate gas side was quantitatively determined by measuring the oxygen content in the sweep gas with a quadrupole mass spectrometer (Pfeiffer Omnistar). The mass spectrometer was routinely calibrated by means of commercial calibration gas mixtures.

Membrane permeation

Permeation experiments on disc shaped membranes with a thickness of 1.3 mm were carried out at temperatures between 1,073 K and 1,223 K. The membranes were allowed to equilibrate at constant temperature in air for several hours before measuring the permeation flux. The oxygen partial pressure $p''(O_2)$ of the sweep gas was varied whereas the partial pressure $p'(O_2)$ of the feed gas was kept constant at 0.21 bar in all experiments. After each change of $p''(O_2)$, the membrane was allowed to reach steady state before the permeation flux was measured. However, even in steady state a very slow decrease of the permeation flux at a rate of 1.5 ‰ per hour was observed. The reason for the degradation is not yet known; X-ray diffraction and EDS analysis of the membranes after the permeation experiments did not yield any evidence for the formation of new phases, which rules out decomposition of the oxide. Since the flux decreased at a constant rate, it was possible to correct the permeation data for this temporal decline.

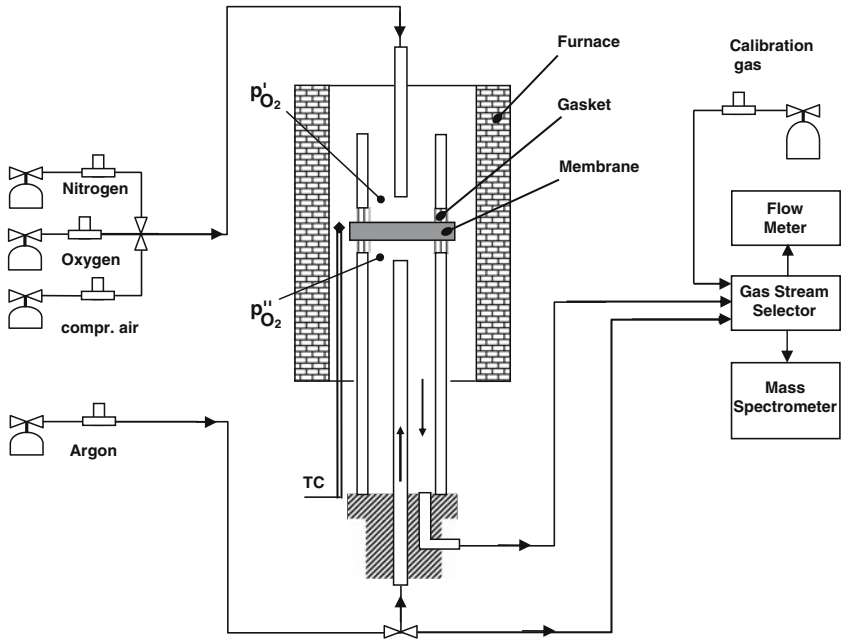

Fig. 2 Cross-sectional view of the membrane permeator including peripheral gas supply and analysis devices

The corrected data are shown in Fig. 3. The relative error of all permeation data was estimated to be equal or lower than 14%.

It is noted that the oxygen permeation flux assumes large values already at small oxygen partial pressure gradients but appears to level out at smaller oxygen partial pressures $p''(O_2)$. This is in contrast to mixed conducting membranes with perovskite structure, where the oxygen flux is often found to be proportional to $n^{-1} \cdot (p''(O_2)^n - p'(O_2)^n)$ [28, 29] and, therefore grows at an increasing rate with decreasing $p''(O_2)$. The fluxes obtained in this work are lower than those recently determined by Smith and Norby [30] for undoped lanthanum nickelate, which is expected as doping with strontium diminishes the concentration of mobile oxygen interstitials.

Defect and transport model

Defect model of $La_{2-x}Sr_xNiO_{4+\delta}$

In this section, a defect model for $La_{2-x}Sr_xNiO_{4+\delta}$ will be presented. The model will be applied to nonstoichiometry data from Vashook et al. [31], which allows us to calculate dependence on oxygen partial pressure of the defect concentrations of $La_{2-x}Sr_xNiO_{4+\delta}$ with $x = 0.5$. These defect concentrations are required for the modelling of the membrane permeation fluxes, which is subject of the next section.

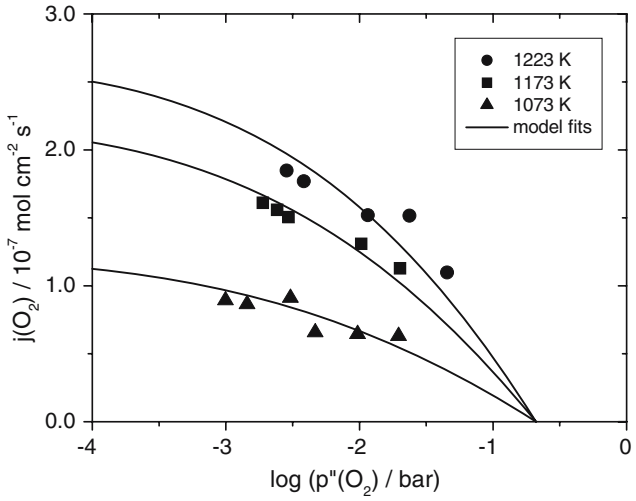

Fig. 3 Experimentally determined oxygen permeation fluxes through a membrane of $La_{2-x}Sr_xNiO_{4+\delta}$ ($x = 0.5$) as a function of the oxygen partial pressure $p''(O_2)$ on the sweep gas side. $p'(O_2)$ was 0.21 bar. Membrane thickness was 1.3 mm. Solid lines indicate fit results obtained from the transport model described in section Flux equations

The defect chemistry of doped $La_{2-x}Sr_xNiO_{4+\delta}$ is dominated by structural defects in the oxygen sublattice. From literature, there is no evidence that any significant amounts of cation defects exist in $La_{2-x}NiO_{4+\delta}$. Likewise, we will assume that in doped $La_{2-x}Sr_xNiO_{4+\delta}$ the substitutional dopant ion is the only cation defect. We will further assume that the dopant ions reside in the lanthanum sublattice only. As, depending on the thermodynamic conditions and the dopant concentration, $La_{2-x}Sr_xNiO_{4+\delta}$ can exhibit either oxygen excess or oxygen deficiency, both oxygen interstitial ions and oxygen vacancies are included as structural anion defects. Although vacancy ordering in the basal plane of the NiO_6 octahedra was observed at room temperature and below [21], there is no evidence of defect ordering at high temperatures. Thus, the vacancies are considered to be randomly distributed over the basal and apical oxygen sites in the perovskite structured layers. As indicated in Fig. 1, the interstitial sublattice consists of tetrahedrally coordinated interstitial sites in the La_2O_2 layers, and the distribution of the oxygen interstitial ions among these sites is also assumed to be random.

If the oxide crystal is in contact with a gas phase, exchange of oxygen at the gas-solid interface may occur through formation/annihilation reactions of oxygen vacancies $V_O^{\cdot\cdot}$ or interstitial ions O_i''. The exchange process may be described by the following reactions:

$$O_O^{\times} + 2Ni_{Ni} \rightleftarrows \frac{1}{2}O_2(g) + 2Ni_{Ni}^{\times} + V_O^{\cdot\cdot} \quad (1)$$

$$O_I'' + 2Ni_{Ni} \rightleftarrows \frac{1}{2}O_2(g) + V_I^{\times} + 2Ni_{Ni}^{\times} \quad (2)$$

In Eqs. 1 and 2, $V_I^{\times}$ denotes an empty interstitial lattice site, and $Ni_{Ni}^{\times}$ and Ni_{Ni} represent Ni^{2+} and Ni^{3+} ions, respectively. Which of these surface reactions prevails, or whether both reactions are effective, is not known. However, for the modelling we will assume that surface exchange occurs only via reaction (1) and that the concentrations of oxygen interstitials and vacancies are coupled via a Frenkel equilibrium reaction:

$$O_O^{\times} + V_I^{x} \rightleftarrows O_I'' + V_O^{\cdot\cdot} \quad (3)$$

Apart from oxidized Nickel ions which are generated in reactions (1) or (2), it is further assumed that also reduced Nickel ions may form via a charge disproportionation of Ni^{2+} to Ni^{3+} and Ni^{+}:

$$2Ni_{Ni}^{\times} \rightleftarrows Ni_{Ni}^{\cdot} + Ni_{Ni}^{\prime} \quad (4)$$

The crystal structure requires that each molecule of stoichiometric La_2NiO_4 consists of two lanthanum lattice sites, one nickel site, four oxygen sites, and two interstitial sites. The nickel sublattice is considered to be free of structural defects and contains only differently charged nickel ions. The sum of the molar fractions of these species yields:

$$[Ni_{Ni}^{\times}] + [Ni_{Ni}^{\cdot}] + [Ni_{Ni}^{\prime}] = 1 \quad (5)$$

The oxygen and interstitial sublattice site balances are given by

$$[O_O^{\times}] + [V_O^{\cdot\cdot}] = 4 \quad (6)$$

$$[V_I^{\times}] + [O_I^{\prime\prime}] = 2 \quad (7)$$

The deviation from stoichiometry of $La_{1.5}Sr_{0.5}NiO_{4+\delta}$ is of the order of 1% of the total oxygen content [31]. It is reasonable to assume that the vacancy and interstitial concentrations are of the same order of magnitude. Therefore, the diluted defect approximation may be applied and Eqs. 6 and 7 are simplified to $[\ O_o^{\times}\ ] \approx 4$ and $[\ V_I^{\times}\ ] \approx 2$. Finally, the electroneutrality condition reads:

$$[Ni_{Ni}^{\cdot}] + 2[V_O^{\cdot\cdot}] = 2[O''_I] + [Ni_{Ni}^{\prime}] + d \quad (8)$$

where d denotes for the molar fraction of the Strontium dopant, $[\ Sr_{La}^{\prime}\ ]$, which is identical to x in $La_{2-x}Sr_xNiO_{4+\delta}$.

For this rather complex defect model, it is difficult to derive explicit equations describing the dependence on oxygen partial pressure dependence of each defect concentration. The treatment is much facilitated if the concentration of one of the defects (in our case this will be the concentration of oxidized nickel, $[\ Ni_{Ni}^{\cdot}\ ]$) is chosen as independent variable and all other defect concentrations as well as the oxygen partial pressure are expressed in terms of this variable. To simplify the following notation, the molar fractions $[\ Ni_{Ni}^{\prime}\ ]$, $[Ni_{Ni}^{\cdot}]$ and $[\ Sr_{La}^{\prime}]$ will be replaced by n, p and d, respectively. The concentration p will be used as independent variable. By taking into account the approximation $[\ O_o^{\times}\ ] \approx 4$ the law of mass action obtained from reaction (1) reads:

$$K_1 = \frac{[Ni_{Ni}^{\times}]^2 \cdot [V_O^{\cdot\cdot}]}{4p^2} \cdot w \quad (9)$$

In Eq. 9, the term $p(O_2)^{1/2}$ has been replaced by w. Likewise, the Frenkel equilibrium (3) and the electronic equilibrium (4) yield:

$$K_F = \frac{[O_I^{\prime\prime}] \cdot [V_O^{\cdot\cdot}]}{8} \quad (10)$$

$$K_{el} = \frac{n \cdot p}{[Ni_{Ni}^{\times}]^2} \quad (11)$$

According to our simplified notation, Eq. 5 is recast into:

$$[Ni_{Ni}^{\times}] = 1 - p - n \quad (12)$$

Inserting Eq. 12 in Eq. 11 and Eq. 9 and rearrangement yields the concentration of reduced nickel ions n and of oxygen vacancies, respectively:

$$n = \frac{2K_{el} \cdot (1-p) + p + \{4K_{el} \cdot p \cdot (1-p) + p^2\}^{1/2}}{2K_{el}} \quad (13)$$

$$[V_O^{\cdot\cdot}] = 4K_1 \cdot \frac{p^2}{(1-p-n)^2} \cdot w^{-1} \quad (14)$$

Furthermore, combination of Eqs. 10 and 14 gives:

$$[O_I^{\prime\prime}] = \frac{K_F}{K_1} \cdot \frac{(1-p-n)^2}{p^2} \cdot w \quad (15)$$

In Eqs. 14 and 15, the concentration of reduced nickel n may be replaced by Eq. 13 in order to obtain expressions in which the concentrations of vacancies and interstitials are functions only of the equilibrium constants K_1, K_F and K_{el} as well as of the independent variable p and the quantity w. The remaining task is therefore to express w as a function of p. We start from the electroneutrality condition (Eq. 8) which may be rewritten as

$$2[O_I^{\prime\prime}] - (p - n - d) - 2[V_O^{\cdot\cdot}] = 0 \quad (16)$$

and insert Eqs. 14 and 15 for $[O_I^{\prime\prime}]$ and $[V_O^{\cdot\cdot}]$. Equation 16 may be recast into a quadratic equation of the form

$$w^2 + \frac{B_2}{B_3} \cdot w + \frac{B_1}{B_3} = 0 \quad (17)$$

where

$$B_1 = -8K_1 \cdot \frac{p^2}{(1-p-n)^2}; \quad B_2 = -(p-n-d);$$
$$B_3 = \frac{2K_F \cdot (1-p-n)^2}{K_1 \cdot p^2} \tag{18}$$

Only one of the two solutions of Eq. 18 is physically meaningful. After re-inserting the quantities B_1, B_2 and B_3, this solution reads:

$$w = \frac{K_1}{4K_F} \cdot \frac{p^2 \cdot (p-n-d+\{(p-n-d)^2+64K_F\}^{1/2})}{(1-p-n)^2} \tag{19}$$

The set of Eqs. 13–15 and 19 may be used to calculate n, $[O_I^{''}]$, $[V_o^{''}]$, and $p(O_2) = w^2$ for a chosen range of concentration p. From the concentrations of interstitials and vacancies, the deviation from stoichiometry is obtained as:

$$\delta = [O_I^{''}] - [V_O^{\cdot\cdot}] = \frac{K_F}{K_1} \cdot \frac{(1-p-n)^2}{p^2} \cdot w - 4K_1 \cdot \frac{p^2}{(1-p-n)^2} \cdot w^{-1} \tag{20}$$

Equation 20 in conjunction with Eqs. 13 and 19 may be used to fit experimental data of δ in $La_{2-x}Sr_xNiO_{4+\delta}$, which yields the unknown constants K_1, K_F and K_{el} (see section Results and discussion).

Flux equations

If a metal oxide is exposed to a gradient of oxygen chemical potential, migration of cations, oxygen and electronic charge carriers may occur in general. To date, no experimental data on cation migration in oxides with the K_2NiF_4 structure are available. However, in perovskite-structured oxides, cation diffusion coefficients determined so far are several orders of magnitude lower than the oxygen diffusion coefficient, and the close proximity of perovskite and K_2NiF_4 structure may lead to the conclusion that this is also true in the case of $La_{2-x}Sr_xNiO_{4+\delta}$. If the cations are considered to be immobile, the cation lattice can be used as a reference system for the oxygen flux in a gradient of oxygen chemical potential. Then, only the fluxes of the oxygen defects and the electronic defects with respect to the lattice need to be considered. In contrast to cubic perovskite-structured oxides, the oxide-ion conductivity in the lanthanum nickel oxides is anisotropic due to their layered crystal structure. Parallel to the (a,b) planes of the structure, oxygen migration can occur via oxygen interstitials inside the La_2O_2 rocksalt layers and via oxygen vacancies in the NiO_6 octahedra. The oxide-ion conductivity parallel to the layers is then given by the sum of the conductivities of each layer:

$$\sigma_O^{\parallel} = \sigma_V^{\parallel} + \sigma_I \tag{21}$$

$\sigma_V^{\parallel}$ stands for the conductivity of vacancies that migrate along the (a,b) plane in the NiO_6 octahedra, whereas σ_I denotes the conductivity of interstitials in the La_2O_2 layers. By taking into account that both $La_2NiO_{4+\delta}$ and $La_{2-x}Sr_xNiO_{4+\delta}$ are prevailing electronic conductors for which $\sigma_O \ll \sigma_e$ holds, the total parallel flux $j(O_2)^{\parallel}$ is written as:[1]:

$$j(O_2)^{\parallel} = -\frac{1}{16F^2} \cdot (\sigma_V^{\parallel} + \sigma_I) \nabla\mu(O_2) \tag{22}$$

The oxygen transport perpendicular to the layers may be subdivided in two coupled processes: (a) Vacancy assisted oxygen migration inside the perovskite-structured layers along the c-axis of the K_2NiF_4 structure, and (b) migration of interstitial oxygen ions across the rocksalt-structured La_2O_2 layers. By using $\sigma_O^{\perp}$ to denote the oxide-ion conductivity perpendicular to the layers, the overall oxygen flux in this direction may be written as:

$$j(O_2)^{\perp} = -\frac{1}{16F^2} \cdot \sigma_O^{\perp} (\nabla_P\mu(O_2) + \nabla_{RS}\mu(O_2)) \tag{23}$$

$\nabla_P\mu(O_2)$ and $\nabla_{RS}\mu(O_2)$ denote the oxygen chemical potential gradients inside the perovskite-structured layer and the rocksalt-structured layer in c-direction, respectively. The partial fluxes inside the different layers may be defined as:

$$j_P(O_2)^{\perp} = -\frac{1}{16F^2} \cdot \sigma_V^{\perp} \nabla_P\mu(O_2) \tag{24}$$

$$j_{RS}(O_2)^{\perp} = -\frac{1}{16F^2} \cdot \sigma_I^{\perp} \nabla_{RS}\mu(O_2) \tag{25}$$

where $\sigma_V^{\perp}$ is the conductivity of vacancies in the NiO_6 octahedra and $\sigma_I^{\perp}$ is the interstitial ion conductivity in the La_2O_2 layers. By assuming that the overall oxygen

[1] In the following derivation we will assume that the oxygen surface exchange reactions are sufficiently fast which means that the overall transport process is limited by bulk migration of oxygen.

transport process is in steady state, the continuity condition requires the partial fluxes in both layers to be equal, and from Eqs. 24 and 25 one obtains

$$\sigma_V^{\perp}\nabla_P\mu(O_2) = \sigma_I^{\perp}\nabla_{RS}\mu(O_2) \tag{26}$$

Combination of Eqs. 23 and 26 yields:

$$j(O_2)^{\perp} = j_P(O_2)^{\perp} = -\frac{1}{16F^2}\cdot\sigma_O^{\perp}\left(\frac{\sigma_V^{\perp}}{\sigma_I^{\perp}}+1\right)\nabla_P\mu(O_2) \tag{27}$$

From a comparison of Eqs. 24 and 27 one obtains:

$$\sigma_O^{\perp} = \frac{\sigma_V^{\perp}\cdot\sigma_I^{\perp}}{\sigma_V^{\perp}+\sigma_I^{\perp}} \tag{28}$$

Bassat et al. [27] found that in $La_2NiO_{4+\delta}$ at 1,173 K, oxygen tracer diffusion parallel to the layers is about two orders of magnitude larger than perpendicular to the layers. This indicates that the transfer of oxygen from one perovskite layer to the other, which involves interstitial migration inside the rocksalt-structured layer, is much more facile than the transport via oxygen vacancies inside the perovskite layers, which is therefore the rate determining step in the overall oxygen transport perpendicular to the layers. By assuming $\sigma_V^{\perp} \ll \sigma_I^{\perp}$ Eq. 23 is simplified to

$$j(O_2)^{\perp} \approx -\frac{1}{16F^2}\cdot\sigma_V^{\perp}\nabla\mu(O_2) \tag{29}$$

Experimentally, the oxygen fluxes parallel and perpendicular to the layers, as given in Eqs. 22 and 29, could only be distinguished by measurements with single-crystalline membranes. However, such measurements would require single crystals of sufficient size which are not readily available. The situation is different if a polycrystalline membrane is considered. In this case, both parallel and perpendicular fluxes contribute to the experimentally accessible total flux. However, the formal treatment is simplified by the fact that the oxygen migration is strongly anisotropic [27]. The following assumptions are made for the derivation of the permeation flux in a polycrystalline membrane:

(I) Within an individual grain, the oxide ions migrate only parallel to the layers of the K_2NiF_4-structure, either via interstitials inside the rocksalt-structured layers, or via vacancies inside the perovskite-structured layers. The ion transfer across the layers can be neglected.

(II) The membrane consists of randomly oriented grains whose average diameter is much smaller than the membrane thickness.

(III) The grain boundaries neither resist nor enhance the migration process.

According to assumption I, the permeation flux through the polycrystal may be described by Eq. 22, but the conductivities $\sigma_V^{\parallel}$ and σ_I must be replaced by effective conductivities. The reason is that in a single crystal, the layers form a straight path throughout the crystal, whereas the migration in a polycrystalline material follows a tortuous path, as the layers in each individual grain have a different orientation. For the permeation flux in a polycrystal, one obtains

$$j(O_2) \approx -\frac{1}{16F^2}\cdot\left(\sigma_V^{*}+\sigma_I^{*}\right)\nabla\mu(O_2) \tag{30}$$

where σ_V^{*} and σ_I^{*} denote the effective conductivities due to vacancy migration and interstitial migration parallel to the layers. As both layers are aligned parallel to each other, the pathways of vacancies and interstitial ions are expected to exhibit the same tortuosity. One may introduce a tortuosity factor which describes the reduction of both σ_V^{*} and σ_I^{*} with respect to the conductivities $\sigma_V^{\parallel}$ and σ_I of the single crystal:

$$\sigma_V^{*} = \tau\cdot\sigma_V^{\parallel} \quad \sigma_I^{*} = \tau\cdot\sigma_I \tag{31}$$

The tortuosity factor τ was calculated by Ormrod and Kirk [32] for cation diffusion in the β'' alumina structure. τ was shown to depend on the grain size and approaches a value of 0.68 for the case of a small grained polycrystal. The ratio of tracer diffusion coefficients determined from polycrystalline $La_2NiO_{4+\delta}$ and those obtained for the oxygen diffusion parallel to the (a,b) plane in single crystals [27] is in good agreement with this value.

The total oxygen flux through a polycrystalline membrane of thickness L, which is exposed to an oxygen partial pressure $p(O_2)_0$ on one side and to $p(O_2)_L$ on the other, can now be obtained from integration of Eq. 30. By taking into account that $\mu(O_2) = \mu^{o}(O_2) + RT\cdot\ln(p(O_2)/p^{o})$, it follows that

$$j(O_2) = -\frac{A}{L}\cdot\int_{\ln p(O_2)_0}^{\ln p(O_2)_L}\left(\sigma_V^{*}+\sigma_I^{*}\right)d\ln p(O_2) \tag{32}$$

where $A = RT/(16\ F^2)$. The conductivities may be expressed in terms of effective defect mobilities u_V^{*} and

u_I^* and the defect concentrations c_V and c_I, respectively:

$$\sigma_V^* = z_O F u_V^* c_V = z_O F u_V^* \cdot \frac{[V_O^{\cdot\cdot}]}{V_m} \tag{33}$$

$$\sigma_I^* = z_I F u_I^* c_I = z_I F u_I^* \cdot \frac{[O_i'']}{V_m} \tag{34}$$

V_m is the molar volume of the oxide. By neglecting the weak concentration dependence of u_V^* and u_I^*, and by substituting w^2 for $p(O_2)$ as in section Defect model of $La_{2-x}Sr_x NiO_{4+\delta}$, the oxygen flux is obtained from Eqs. 32–34 as:

$$\begin{aligned} j(O_2) = &-\frac{A}{L}\cdot\frac{2z_V F u_V^*}{V_m}\cdot\int_{w_0}^{w_L}\frac{[V_O^{\cdot\cdot}]}{w}\mathrm{d}w \\ &-\frac{A}{L}\cdot\frac{2z_I F u_I^*}{V_m}\cdot\int_{w_0}^{w_L}\frac{[O_i'']}{w}\mathrm{d}w \end{aligned} \tag{35}$$

In the previous section, the concentrations $[V_{;O}^{\cdot\cdot}]$ and $[O_{;I}^{''}]$ as well as the oxygen partial pressure related quantity w have been derived as a function of the concentration of electron holes, p. The derivative dw with respect to p may be obtained from Eq. 19:

$$\begin{aligned} \mathrm{d}w = -\frac{K_1 K_{el}}{4K_F}\cdot\Bigg\{&\left(p-n-d+\{(p-n-d)^2+64K_F\}^{1/2}\right) \\ &\cdot\left(\frac{1}{2n}+\frac{p}{n^2}\cdot\Gamma(p)\right) \\ &+\frac{p}{n}\cdot\left(1+\frac{\Gamma(p)}{2K_{el}}\right)\cdot\left(\frac{p-n-d}{\{(p-n-d)^2+64K_F\}^{1/2}}\right)\Bigg\} \end{aligned} \tag{36}$$

$$n = \frac{2K_{el}\cdot(1-p)+p+\{4K_{el}\cdot p\cdot(1-p)+p^2\}^{1/2}}{2K_{el}} \tag{37}$$

$$\Gamma(p) = \frac{2K_{el}+p(1+4K_{el})}{\{4K_{el}\cdot p\cdot(1-p)+p^2\}^{1/2}} \tag{38}$$

Equations 14, 15, 19 and 36–38 may be inserted into Eq. 35, and after integration the oxygen flux is obtained as a function only of the independent concentration p. While still being an analytical expression, the resulting equation is rather complex and will not be reported here.

Results and discussion

The only investigation known to the authors in which the deviation from stoichiometry of strontium doped lanthanum nickelate has been determined in situ as a function of oxygen partial pressure and temperature was conducted by Vashook et al. [31]. The data were measured by means of coulometric oxygen[2]. It was found that within the range of oxygen partial pressures for which δ was measured, the oxide was hyperstoichiometric except for temperatures $T > 1{,}373$ K and under reducing conditions. Figure 4 displays the experimentally determined oxygen content of $La_{2-x}Sr_xNiO_{4+\delta}$ ($x = 0.5$) at 1,223 K. The data were fitted with Eq. 20 which was derived in section Defect model of $La_{2-x}Sr_xNiO_{4+\delta}$. The fit result is indicated by a solid line.

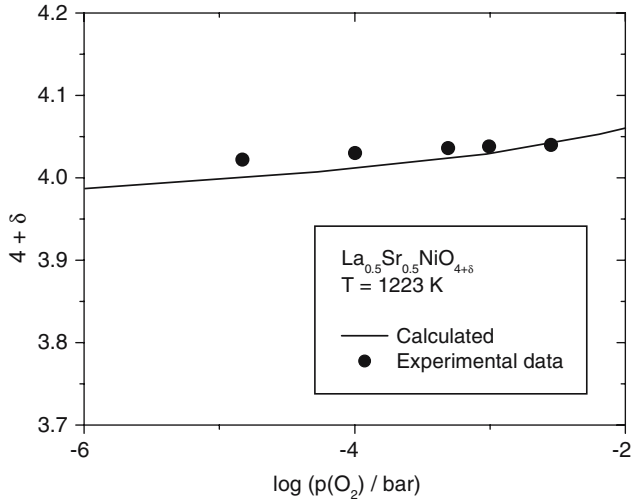

Fig. 4 Oxygen content of $La_{2-x}Sr_xNiO_{4+\delta}$ ($x = 0.5$) as a function of the oxygen partial pressure for $T = 1{,}223$ K. Experimental data taken from [31]

The quality of the fit is fair, given the small number of data points and the small range of oxygen partial pressures for which data are available. At low oxygen partial pressures, the model calculation slightly underestimates the oxygen content and has a larger slope than the experimental data. Essentially the same trend is found when experimental data and the corresponding fits for 1,073 and 1,173 K are compared. The fit results were nearly independent of the choice of the equilibrium constant K_{el} of the electronic equilibrium, except if a very large value was assumed for K_{el} In this case the fit quality was diminished. The fit is essentially dependent on only two fit parameters, which are the surface oxygen exchange equilibrium constant K_1 and Frenkel equilibrium constant K_F. Table 1 summarizes the equilibrium constants calculated from the fits.

[2] The initial oxygen content of the samples was determined by thermogravimetric measurements of the weight change in flowing hydrogen.

Table 1 Equilibrium constants for the external oxygen exchange reaction, oxygen Frenkel reaction and electronic equilibrium reaction

Temperature (K)	K_1	K_F	K_{el}
1,073	$(1.1 \pm 0.3) \cdot 10^{-7}$	$(4.1 \pm 1.5) \cdot 10^{-8}$	$\{2 \cdot 10^{-3}\}$
1,173	$(9.0 \pm 3.4) \cdot 10^{-7}$	$(2.7 \pm 0.9) \cdot 10^{-7}$	$\{4 \cdot 10^{-4}\}$
1,223	$(4.6 \pm 2.1) \cdot 10^{-6}$	$(9.2 \pm 3.5) \cdot 10^{-7}$	$\{2 \cdot 10^{-6}\}$

Results for K_{el} are given in parentheses to indicate the large uncertainty of the values

As expected, charge compensation of the acceptor dopant occurs mainly by oxidized nickel ions, which are the dominant electronic defect species. The large Ni^{3+} concentration accounts for the high p-type conductivity of about 70 S cm^{-1} observed for $La_{1.5}Sr_{0.5}NiO_{4+\delta}$ at this temperature [31]. The total conductivity was found to decrease slightly with decreasing $p(O_2)$, which is consistent with the decreasing concentration of Ni^{3+}, as shown in Fig. 5. On the other hand, the electron concentration bears a large uncertainty due to the insensitivity of the fits with respect to a variation of K_{el}. The concentration may be much lower, however, a larger electron concentration than is shown in Fig. 5 can be ruled out as the fit quality deteriorated when a larger K_{el} was assumed.

At high oxygen partial pressures, the oxygen stoichiometry is predominantly determined by the number of oxygen interstitials. A crossover of the interstitial and vacancy concentration is observed at about $p(O_2) \approx 10^{-5}$ bar. The oxide is stoichiometric at this point, and becomes oxygen deficient below this oxygen partial pressure. For 1,173 K, the stoichiometric point is reached at $p(O_2) \approx 10^{-6}$ bar, and for 1,073 K at $p(O_2) \approx 10^{-7}$ bar. It is noted, however, that due to the deviation of the fit from the experimental data, either the vacancy concentration is overestimated or the interstitial concentration is underestimated. In both cases, the calculated crossover oxygen partial pressure displayed in the Kröger–Vink diagram would be too large.

The calculated defect concentrations and the mass action constants reported in Table 1 may now be used to fit the permeation fluxes obtained in this work. The set of Eqs. 35–38 is employed for this purpose.

Equation 35 contains the effective mobilities u_I^* and u_V^* of the interstitials and vacancies as fit parameters. It was observed that the quality of the fits was nearly independent of the value of the vacancy mobility u_V^*. Only if unreasonably high values for u_V^* were assumed, the fits were affected in the range of $p(O_2)$ in which experimental data are available. The Kröger–Vink diagram (Fig. 5) shows that the vacancy concentration in this range is at least one order of magnitude smaller than the interstitial concentration. Therefore, the contribution of oxygen migration via vacancies to the permeation flux is small. This makes it impossible to obtain reliable values of the vacancy mobility. Consequently, u_V^* was set to zero and only the interstitial mobility u_I^* was used as parameter in the fit calculations. The fit result for 1,223 K are displayed as solid line in Fig. 6. The corresponding fit results for 1,073 and 1,173 K are shown in Fig. 7.

The partial fluxes of oxygen interstitials and vacancies shown in Figs. 6 and 7 were calculated to

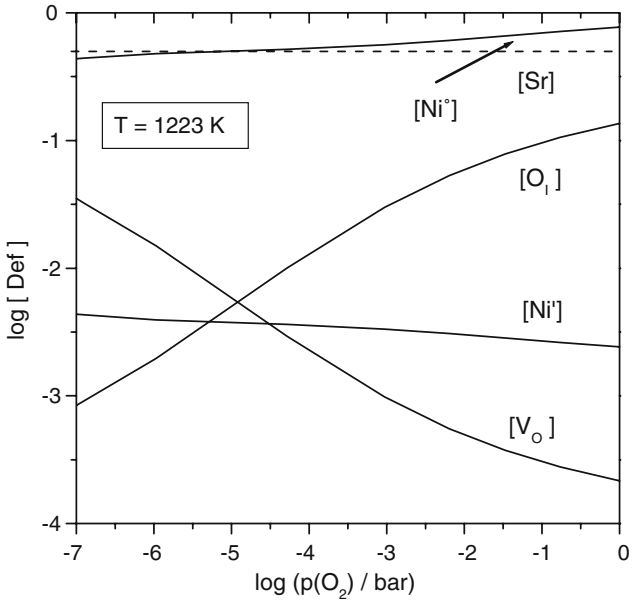

Fig. 5 Kröger–Vink diagram for $La_{2-x}Sr_xNiO_{4+\delta}$ ($x = 0.5$) at 1,223 K

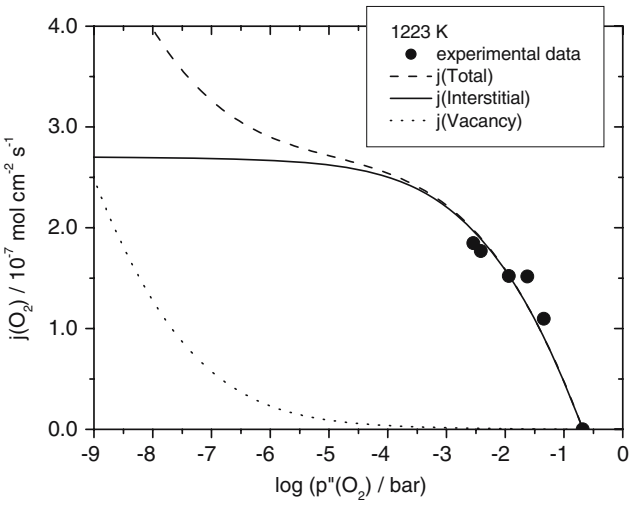

Fig. 6 Total permeation flux and partial fluxes of interstitials and vacancies in $La_{2-x}Sr_xNiO_{4+\delta}$ ($x = 0.5$) at $T = 1{,}223$ K, calculated for $u_V^* = u_I^*$

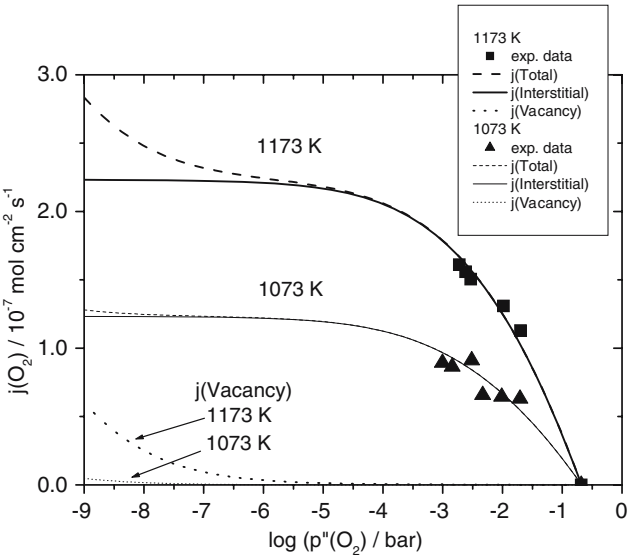

Fig. 7 Total permeation flux and partial fluxes of interstitials and vacancies in $La_{2-x}Sr_xNiO_{4+\delta}$ ($x = 0.5$) at $T = 1{,}073$ K and 1,173 K, calculated for $u_V^* = u_I^*$

demonstrate how a non-negligible transport of oxygen via oxygen vacancies would affect the permeation flux through a membrane of $La_{1.5}Sr_{0.5}NiO_{4+\delta}$. For this, a hypothetical vacancy mobility ($u_V^* = u_I^*$) was assumed. The oxygen partial pressure dependence of the partial fluxes is quite different. With increasing gradient of oxygen partial pressure, the interstitial flux quickly rises to fairly large values but remains constant for larger gradients. The reason for this behaviour lies in the interstitial concentration which decreases with $p''(O_2)$. This causes the partial conductivity due to interstitial migration to decrease, while the driving force increases at the same time. The opposite situation is met with the partial conductivity due to vacancy migration, which increases with decreasing oxygen partial pressure, since the vacancy concentration is small at high oxygen partial pressures and increases with decreasing $p(O_2)$. Thus, oxygen transport via vacancies would contribute significantly to the oxygen flux only at low $p''(O_2)$ but would grow with decreasing $p''(O_2)$ at an increasing rate. The onset of the vacancy-mediated permeation flux is found at about the same oxygen partial pressure as the cross-over of vacancy and interstitial concentration (cf. Fig. 5). It is obvious from Figs. 6 and 7 that additional experimental data at lower $p''(O_2)$ would be required to verify a possible vacancy contribution to the permeation flux.

The effective mobility of the interstitials u_I^* which was obtained from the fits shows an Arrhenius-type behaviour, as indicated in Fig. 8.

The activation energy (E_a = 80.5 kJ/mol) obtained from this plot is identical to the enthalpy of migration of the interstitial ions. This value may be compared with activation energies obtained from tracer diffusion measurements, provided the enthalpy of formation of the interstitials is known. Data of the deviation from stoichiometry [31] indicate only a weak temperature dependence of δ in $La_{1.5}Sr_{0.5}NiO_{4+\delta}$ in the temperature range considered here. An estimation of the interstitial formation enthalpy from these data yields $\Delta_f H_m = -11\,\mathrm{kJ\,mol^{-1}}$. The activation energy of the oxygen diffusion results from the sum of the interstitial migration enthalpy and the interstitial formation enthalpy, and a value of 69.5 kJ mol^{-1} is obtained. This is somewhat lower than the value of 86.8 kJ mol^{-1} reported by Bassat et al. [27] for oxygen tracer diffusion in polycrystalline $La_2NiO_{4+\delta}$ in the temperature range 773–1,073 K. Skinner et al. [33, 34] obtained E_A = 82 kJ mol^{-1} for the undoped oxide, and E_A = 55kJ mol^{-1} for $La_{2-x}Sr_xNiO_{4+\delta}$ with $x = 0.1$. For $x = 0.2$, the activation energy seems to be larger than for $x = 0.1$, however, due to the large scatter of the diffusion coefficients reported by these authors, no clear conclusion can be drawn regarding the dependence of the activation energy on the strontium content. Nevertheless, it appears that increasing the dopant content tends to reduce the activation energy.

A more significant conclusion derives from the oxygen tracer diffusion measurements in single-crystalline $La_2NiO_{4+\delta}$ carried out by Bassat et al. [27]. The authors obtained a small activation energy of 21.2 kJ mol^{-1} for the diffusion perpendicular to the (a,b) plane of the K_2NiF_4-structure, and a value of 85 kJ mol^{-1} for the diffusion parallel to this plane. The

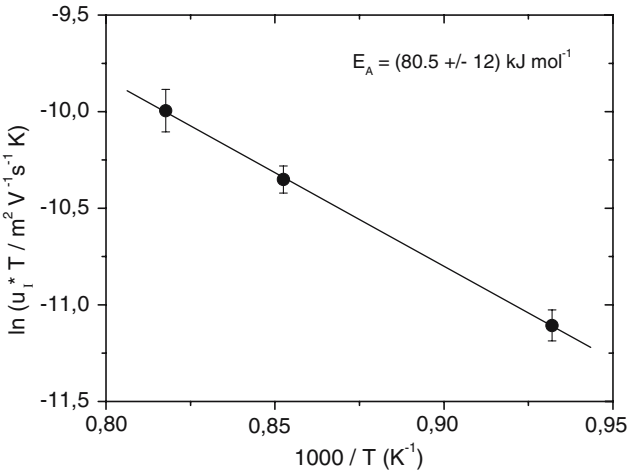

Fig. 8 Arrhenius plot of the effective interstitial ion mobility of $La_{2-x}Sr_xNiO_{4+\delta}$ ($x = 0.5$)

latter value is close to E_A = 69.5 kJ mol^{-1} determined for $La_{1.5}Sr_{0.5}NiO_{4+\delta}$ in the present work, particularly if it is assumed that E_A decreases with increasing dopant content. The samples used by Bassat et al. had large oxygen excess (δ = 0.14) which suggests that oxygen interstitials were the prevailing structural defect species. Thus, the diffusion along the (*a*,*b*)-plane can be mainly attributed to oxygen interstitials in the La_2O_2 layers, whereas vacancy diffusion along the perovskite-structured layers is negligible. This supports the results obtained earlier in this section, from which it may be concluded that the permeation flux in $La_{1.5}Sr_{0.5}NiO_{4+\delta}$ is also dominated by oxygen interstitial migration in the La_2O_2-layers.

The small activation energy found for oxygen diffusion perpendicular to the (*a*,*b*)-plane in $La_2NiO_{4+\delta}$ was explained by a charge transfer from doubly charged oxygen interstitials to nickel ions, whereby singly charged interstitials (O^-) are formed which then migrate via vacancies on equatorial oxygen sites in the perowskite-type layers [27]. In order to keep our model calculations simple, we did not include differently charged oxygen interstitial species in our defect model. Therefore, the existence of O^- interstitials can neither be confirmed nor ruled out, as no significant contribution of vacancy-assisted migration of oxygen was found in the oxygen partial pressure range for which experimental data are available. However, the model calculations suggest that vacancy-assisted oxygen migration might be observed if permeation data would be collected at lower oxygen partial pressures on the oxygen lean side of the membrane. This conclusion must await confirmation from further experiments.

Conclusions

The aim of this study was to investigate the contribution of structural oxygen defects to oxygen transport in acceptor doped lanthanum nickelates. A defect chemical model was used to calculate the defect concentrations in $La_{1.5}Sr_{0.5}NiO_{4+\delta}$ at different temperatures and oxygen partial pressures and to experimental results for the permeation through $La_{1.5}Sr_{0.5}NiO_{4+\delta}$ membranes. From the modelling the following conclusions were obtained:

(1) Doubly charged oxygen interstitials and oxidized nickel ions (Ni^{3+}) are the dominating defect species in $La_{1.5}Sr_{0.5}NiO_{4+\delta}$ in oxidizing conditions at temperatures between 1,073 K and 1,223 K. The concentration of oxygen vacancies cannot be neglected and grows with decreasing oxygen partial pressure, whereas the oxygen interstitial concentration decreases. At 1,223 K the oxide becomes stoichiometric at $p(O_2) = 10^{-5}$ bar. With decreasing temperature, the oxygen partial pressure of the stoichiometric point shifts towards smaller values. At 1,073 K it is found at $p(O_2) = 10^{-7}$ bar. Below this oxygen partial pressure, the oxide becomes oxygen deficient.

(2) A contribution of oxygen transport via vacancies to the permeation flux through $La_{1.5}Sr_{0.5}NiO_{4+\delta}$ could not be verified. The reason may be that either the vacancies are not mobile enough or that the permeation was measured under too oxidizing conditions at which the vacancy concentration is too small to make a significant contribution to the transport of oxygen. In order to solve this question, permeation measurements in an extended oxygen partial pressure range are required and will be presented in due course.

(3) The activation energy of the interstitial mobility in $La_{1.5}Sr_{0.5}NiO_{4+\delta}$ was determined to be 80.5 ± 12 kJ mol^{-1}, from which a value of 69.5 kJ mol^{-1} is calculated for the activation energy of the oxygen diffusion. This value is somewhat lower than the activation energy E_a = 86.8 kJ mol^{-1} obtained from oxygen diffusion data of polycrystalline $La_2NiO_{4+\delta}$, but much larger than the activation energy for oxygen diffusion perpendicular to the layers of the K_2NiF_4 structure. This is another strong indication that the oxygen transport in $La_{1.5}Sr_{0.5}NiO_{4+\delta}$ occurs predominantly via oxygen migration parallel to the layers of the structure.

Acknowledgements The authors are grateful for financial support from the Deutsche Forschungsgemeinschaft (Research grants DFG MS611/2-1 and DFG MS611/2-2).

References

1. Bednorz JG, Müller KA (1986) Z Phys B64:189
2. Tranquada JM (1998) Physics and chemistry of materials with low-dimensional structures 20 (neutron scattering in layered copper-oxide superconductors) p 225
3. Matsuda M, Fujita M, Yamada K, Birgeneau RJ, Kastner MA, Hiraka H, Endoh Y, Wakimoto S, Shirane G (2000) Phys Rev B 62(13):9148
4. Klauss HH, Baabe D, Mienert D, Birke M, Luetkens H, Litterst FJ, Huecker M, Buechner B, Cheong SW (2002) Hyperfine Inter 136(137):711
5. Bourges P, Sidis Y, Braden M, Nakajima K, Tranquada JM (2003) Phys Rev Lett 90(14):147202/1
6. Freeman PG, Boothroyd AT, Prabhakaran D, Enderle M, Niedermayer C (2004) Phys Rev B 70(2):024413/1
7. Freeman PG, Boothroyd AT, Prabhakaran D, Lorenzana J (2005) Los Alamos National Laboratory, Preprint Archive, Condensed Matter 1

8. Kakol Z, Spalek J, Honig JM (1989) J Solid State Chem 79(2):288
9. Sreedhar K, Honig JM (1994) J Solid State Chem 111(1):147
10. Kanai M, Matsuura D, Kawai T, Miki H (1997) Physica C 289(3&4):223
11. Wu G, Neumeier JJ (2003) Phys Rev B 67(12):125116/1
12. Daroukh AL M, Vashook VV, Ullmann H, Tietz F, Arual raj I (2003) Solid State Ionics 158(1,2):141
13. Kharton VV, Viskup AP, Kovalevsky AV, Naumovich EN, Marques FMB (2001) Solid State Ionics 143(3–4):337
14. Vashook VV, Trofimenko NE, Ullmann H, Makhnach LV (2000) Solid State Ionics 131(3–4):329
15. Vashook VV, Yushkevich II, Kokhanovsky LV, Makhnach LV, Tolochko SP, Kononyuk IF, Ullmann H, Altenburg H (1999) Solid State Ionics 119(1– 4):23
16. Kharton VV, Viskup AP, Naumovich EN (1999) J Mater Chem 9:2623
17. Jorgensen JD, Dabrowski B, Pei S, Richards DR, Hinks DG (1989) Phys Rev B 40(4):2187
18. Paulus W, Cousson A, Dhalenne G, Berthon J, Revcolevschi V, Hosoya S, Treutmann W, Heger G, Le Toquin R (2002) Solid State Sciences 4(5):565
19. RICE DE, Buttrey DJ (1993) J Solid State Chem 105:197
20. Tamura H, Hayashi A, Ueda V (1996) Physica C 258(1&2):61
21. Medarde M, Rodriguez-Carvajal J (1997) Z Phys B 102(3):307
22. Skinner SJ (2003) Solid State Sciences 5(3):419
23. Hucker M, Chung K, Chand M, Vogt T, Tranquada JM, Buttrey DJ (2004) Phys Rev B 70(6):064105/1
24. Ishikawa K, Shibata W, Watanabe K, Isonaga T, Hashimoto M, Suzuki Y (1997) J Solid State Chem 131(2):275
25. Minervini L, Grimes RW, Kilner JA, Sickafus KE (2000) J Mater Chem 10(10):2349
26. Frayret C, Villesuzanne A, Pouchard M (2005) Chem Mater 17(26):6538
27. Bassat JM, Odier P, Villesuzanne A, Marin C, Pouchard M (2004) Solid State Ionics 167(3–4):341
28. Bouwmeester HJM, Burggraaf AJ (1996) In Burggraaf AJ, Cot L (eds) Dense ceramic membranes for oxygen separation, Fundamentals of inorganic membrane science and technology. Elsevier Science B.V. p 435
29. Huang KQ, Schroeder M, Goodenough JB (1999) Proceedings of the international symposium ''Solid State Ionic Devices'', Proc. Electrochem. Soc. PV 99-13, p 95
30. Smith JB, Norby T (2006) J Electrochem Soc 153(2):A233
31. Vashook VV, Tolochko SP, Yushkevich II, Makhnach LV, Kononyuk IF, Altenburg H, Hauck J, Ullmann H (1998) Solid State Ionics 110(3–4):245
32. Ormrod SE, Kirk DL (1978) Physica Status Solidi A 50(2):K193
33. Skinner SJ, Kilner JA (2000) Solid State Ionics 135(1–4):709
34. Skinner SJ, Kilner JA (1999) Ionics 5:171